Binary mixture adsorbed in a slit pore: Field-induced population inversion near the bulk instability

C. Brunet, J. G. Malherbe, and S. Amokrane
Physique des Liquides et Milieux Complexes, Faculté des Sciences et Technologie, Université Paris Est (Créteil), 61 av. du Général de Gaulle, 94010 Créteil Cedex, France
(Received 31 May 2010; published 11 August 2010)

The recently proposed method for modulating through an external field the composition of a binary fluid mixture adsorbed in a slit pore is discussed. The population inversion near the bulk (demixing) instability is first analyzed in the case of a symmetric mixture of nonadditive hard spheres, without field. It is next investigated for a mixture comprising dipolar particles subject to an external field. The influence of several factors on the adsorption curves including bulk composition, pore width, field direction, polarizability versus permanent dipoles, and temperature on this field induced population inversion is shown by Monte Carlo simulation.

DOI: 10.1103/PhysRevE.82.021504 PACS number(s): 64.75.Xc, 82.70.Dd, 68.43.−h

I. INTRODUCTION

When a porous material is put in contact with a bulk fluid, most of its properties—mechanical, electrical, optical, etc.—are modified by the fluid that adsorbs in the pores. The question of the control of the associated physical parameters—viscosity, conductivity, permittivity, etc.—is thus of considerable practical interest in materials science. More generally, understanding the factors that regulate the adsorption process—composition of the adsorbing fluid, adsorption geometry, various interactions, etc.—is important in domains ranging from separation processes to nanotechnology [1]. Of course, different methods have been developed to control the behavior of the adsorbed fluid for specific needs and a vast literature exists on these questions. In the case of a pore in equilibrium with a bulk mixture, we have recently proposed [2] a method for modulating the composition of the adsorbed fluid that combines three mains characteristics: (1) the control is through an external field. (2) It leaves the thermodynamic state of the bulk fluid unmodified. (3) It is based on generic mechanisms. Concerning point (1) we considered the action of an external field that couples with the particles (here their dipole moment). This was partly motivated by the experiments of Marr *et al.* [3–5] on polystyrene spheres with a diameter of about 3μ, confined between two planar conducting surfaces. These authors have shown that the structuring of the confined fluid depends on the separation between the plates or the strength of the applied field. Combining this geometrical confinement plus external field with the presence of several species is expected to allow an even greater control of the state of the confined fluid. We thus considered a mixture in which one species bears a dipole moment, permanent or induced, that interacts with a uniform external field (produced for example by two parallel metallic plates as in the device of Marr *et al.* This may also be to a magnetic field, for ferrocolloids). About point (2) now, it is clear that the possibility to control the pore filling at fixed bulk state would greatly facilitate applications in comparison with standard adsorption methods based on a change in bulk thermodynamic variables, such as the pressure or the density. The same holds with point (3)—generic mechanisms—since a control that does not rely on a subtle combination of specific interactions should be robust and feasible with simpler components. We thus choose to point out the basic mechanism on a simple model with only hard sphere and dipolar interactions and perfectly smooth pore walls. The physical situation closest to this model is then the adsorption of colloids (see for example [6]), in contrast with molecular adsorption in which specificity is important (see for, e.g., [7,8] and Ref. [9] for more recent work). One additional advantage of the former is the possibility to tune their effective interaction (e.g., by adding polymeric depletants) and their coupling with external fields, in confined geometry [10]. This makes them more flexible candidates than molecular systems for the realization of the optimum conditions for the proposed method.

Finally, a study by analytical approaches usually involves approximations whose effect might be difficult to estimate. Even for the crude model we consider here, we indeed have to deal with an inhomogeneous asymmetric mixture, anisotropic interactions, variable number of particles, etc. We thus used computer simulations. Since a complete study of the pore/binary mixture equilibrium would then be prohibitive, we will focus on the new mechanism presented rapidly in our previous work [2]. We choose the Monte Carlo method, more convenient than molecular dynamics in the situations we consider that combine anisotropic forces and variable number of particles. The main result we have obtained in Ref. [2] is the possibility to produce, in the pore, a field induced population inversion when the bulk is near (the demixing) instability: we start from the situation of a pore in equilibrium with a bulk mixture having a tendency to demix and widely different concentrations of the two components; when the strength of the field applied in the pore region is varied, a jump in the adsorption of the minority component occurs. After a certain threshold value, the pore becomes filled with this species, while the former majority component simultaneously desorbs. One may accordingly produce a jump in the physical responses mentioned above by the sole action of the external field. A similar effect induced by a variation of the bulk density has been described in Refs. [11,12], but in contrast with these studies, the thermodynamic state of the bulk fluid is here unaffected. As an example, one may induce in this way a field activated revers-

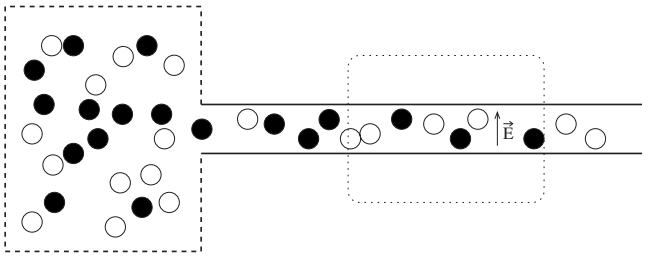

FIG. 1. Schematic representation of the pore/bulk fluid equilibrium. The binary mixture (different species are represented by white and black circles) confined in a slit pore (thick lines) exchanges particles with the bulk fluid (dashed boundary). The region far from the interface (dotted boundary) in which the uniform field is applied is simulated by two parallel walls with separation H and infinite extent in the direction x, y.

ible jump in reflectivity of the porous medium, say for display applications. The objective of this work is to deepen the analysis of this field induced population inversion near the bulk instability (referred to here as the F-PINBI effect) and show how the predictions depend on various parameters: bulk composition, temperature, pore width, field direction, permanent, and induced dipoles. This paper is then organized as follows: in Sec. II, we present the model and detail the methods we used to study it. In Sec. III, we discuss the population inversion first for nonadditive mixtures without dipoles. We next present the results for mixtures with dipolar particles subject to an external field including the influence of the most important parameters. In the conclusion, we consider the possibility to extend the main results to more general confined mixtures.

II. MODELS, METHODS

A. Models

The physical situation we consider is depicted schematically in Fig. 1: a binary mixture confined between two parallel, perfectly smooth walls is in equilibrium with a bulk mixture. This model should be appropriate to a real slitlike pore whose lateral dimensions are much larger than the separation H between the walls and that exchanges particles with a reservoir through an interfacial region much smaller than the remainder of the pore. Since this region plays then a negligible role [13], the fluid in the reservoir away from the interface will be referred to as the "bulk." As in [14] the mixture comprises pure hard-spheres (species 1, diameter σ) and dipolar hard-spheres (species 2, same diameter σ), with a nonadditive diameter σ_{12} in the potential u_{12}^{HS}. A positive nonadditivity will be considered in order to favor demixing in the bulk (a Yukawa repulsive interaction between unlike spheres will also be used to test the sensitivity to this aspect of the model). Both species have a hard-sphere interaction with the walls. A uniform electric field either normal $\boldsymbol{E}=E\boldsymbol{u}_z$ or parallel $\boldsymbol{E}=E\boldsymbol{u}_x$ to the walls is applied in the pore but not in the bulk. This field interacts with the dipole moments $\boldsymbol{\mu}_i$, the latter being either permanent or the ones induced by the local field, as a result of an applied external field.

In recent work, we already pointed out how the structure could be modulated by the combination of various interactions [15,16] and by the action of the field [14]. However, only the density profile of the particles through the pore could be modulated in [14] since the total number of particles was kept fixed (simulations in the canonical ensemble). Here, we consider an open pore to allow variations in the mean composition of the fluid filling the pore and much stronger variations of the density profiles. This simple confinement geometry has been considered in numerous theoretical studies of confined fluids—see for example [7,12,14–19] and references therein. The role of the thermodynamic variables or the action of an external field on the adsorption has also been considered several times. See for, e.g., [17] for the role of the pressure in one-component fluids, or [11,12,18] for the effect of changing the density or the composition in the adsorption from bulk mixtures. Our method differs from these studies since we use an external field as the control parameter. On the other hand, when the latter was present—the field induced filling of a pore was studied for example in [20] (cylindrical) and in [21] (slit)—this concerned only one-component fluids.

In the method we proposed, the novelty resides precisely in the combination of selective field effect (through the coupling with the dipolar species) on the adsorption from a mixture and closeness to the bulk demixing that also favors strong variations in composition in the pore. A field induced PINBI effect triggered by a slight change in the field strength becomes then possible. All the other parameters—pore geometry, interactions (between the particles and the particles and the confining medium) as well as the bulk thermodynamic state remaining fixed, this method constitutes in principle a very flexible way of controlling the state of the adsorbed fluid. In connection with real systems, the choice of a model with purely hard-sphere potential and smooth walls makes this model more appropriate [16] to a mixture of hard-sphere-like colloidal particles, than to a molecular mixture (see however the final remarks). This should always be possible since besides particles having a permanent dipole such as magnetic colloids, colloidal particles are always polarizable to some extent. The possibility to prepare even hollow core shell particles [22] illustrates one possible way of achieving the required difference in polarizability.

B. Methods, simulation details

As explained above, an inhomogeneous multicomponent mixture with anisotropic interactions being difficult to study by analytical methods (see the study by density functional theory of the adsorption from a mixture of polar molecules [23] and of a confined one-component dipolar fluid [24]), we used Monte Carlo simulation (for references on similar simulations of confined dipoles see, for e.g., [14,25–27]). We thus detail below the method we used to study the pore-fluid equilibrium.

1. Simulation strategy

The pore/fluid equilibrium is usually studied by the appropriate version of the Gibbs ensemble Monte Carlo method

TABLE I. Nonadditive hard-sphere mixture.

ρ_b	$\beta\mu_1^{ex}$	$\Delta\beta\mu_1^{ex}$	$\beta\mu_2^{ex}$	$\Delta\beta\mu_2^{ex}$
0.53	4.3792	$\pm 4\times 10^{-4}$	7.948	$\pm 2\times 10^{-3}$
0.54	4.5307	$\pm 6\times 10^{-4}$	8.226	$\pm 3\times 10^{-3}$
0.55	4.6880	$\pm 4\times 10^{-4}$	8.513	$\pm 2\times 10^{-3}$
0.56	4.8482	$\pm 3\times 10^{-4}$	8.801	$\pm 2\times 10^{-3}$
0.57	5.0155	$\pm 3\times 10^{-4}$	9.097	$\pm 2\times 10^{-3}$

TABLE II. Nonadditive dipolar hard-sphere mixture.

ρ_b	$\beta\mu_1^{ex}$	$\Delta\beta\mu_1^{ex}$	$\beta\mu_2^{ex}$	$\Delta\beta\mu_2^{ex}$
0.51	4.0824	$\pm 5\times 10^{-4}$	7.332	$\pm 5\times 10^{-3}$
0.53	4.3745	$\pm 1\times 10^{-3}$	7.85	$\pm 1\times 10^{-2}$
0.54	4.526	$\pm 2\times 10^{-3}$	8.15	$\pm 1\times 10^{-2}$
0.55	4.683	$\pm 7\times 10^{-3}$	8.41	$\pm 1\times 10^{-2}$
0.56	4.845	$\pm 1\times 10^{-3}$	8.69	$\pm 2\times 10^{-2}$

[13] (GEMC). Since we do not attempt here to do a full mapping of the pore/bulk fluid phase diagram we adopted a simpler strategy. The pore/bulk mixture equilibrium is determined by the equality of the chemical potentials μ_1 and μ_2 of the components of the binary mixture, in the bulk and in the pore. This is in principle achieved by explicitly allowing particles exchanges between the pore and the bulk as in the GEMC method.

Here, a combined canonical/grand-canonical simulation, more adapted to our needs was used. Indeed, the practical control variables are the total density ρ_b and mole fractions $x_i^b=N_i/N$, in the bulk. The bulk is thus considered in the canonical ensemble by a (N_1,N_2,V,T) MC simulation. Species 2 is the dipolar one, with a mole fraction x_2^b with $N=N_1+N_2$ the total number of particles and $\rho_b=N/V$ the total density. Note that these overall composition x_2^b and density ρ_b need not necessarily correspond to a homogeneous mixture (the subscript b is used only to distinguish the bulk from the pore). By considering only homogeneous states or metastable states very close to the coexistence boundary, μ_1 and μ_2 in the bulk are determined with sufficient accuracy from Widom's insertion method (see for, e.g., [28] for this point). μ_1 and μ_2 are then used to study the fluid in the pore in the grand-canonical (GC) ensemble, by a (μ_1,μ_2,V,T) MC simulation, where $V=S(H-\sigma)$ is the accessible volume in the pore, with H the pore width and $S=L^2$ the surface of the walls, with periodic conditions in the x and y directions. We can then compute the average density of each species in the pore as a function of ρ_b and x_2. The reduced densities in the pore are $\bar{\rho}_i=\bar{N}_i\sigma^3/V$, with $\bar{N}_i$ the average number of particles of type i for a lateral surface S. The chemical potentials in the bulk are measured with sufficient accuracy after 2^{17} to 2^{20} MC steps (1 step involves the displacement of all the particles and 10^3 insertion trials for each species) depending or not on the presence of dipolar particles. The values of μ_1^{ex} and μ_2^{ex} that were used to obtain Figs. 5 and 7 below are given in Tables I and II. In the pore, the grand-canonical simulation with dipoles involved between 10 000 and 40 000 MC steps for $x_2^b=0.02$ and 50 000 MC steps for $x_2^b=0.04$ (1 step involves translation, rotation—for permanent dipoles-insertion-deletion trials corresponding to the average numbers of all particles). When dipolar particles are considered, reduced variables $E^*=E(\sigma^3/kT)^{1/2}$ and $\mu^*=\mu/(kT\sigma^3)^{1/2}$ will be used (in SI units, σ^3 should be multiplied by a factor $4\pi\epsilon_0$).

The simulation for this model raises two additional questions. The first one, specific to the long-range dipolar interactions will be detailed in the next paragraph. The second one is the treatment of mixtures that are highly asymmetric in composition, typically $x_2=0.02$. For this last point, the main concern is to have sufficiently large volumes (in the bulk) and lateral surfaces (in the pore) to have a significant statistics given the relatively small numbers of particles of the minority species. However, when dealing with dipolar particles, their number N_2 can hardly exceed a few hundreds if the simulation length is to be kept reasonable. The simulations in the bulk are thus done with a box size $L=30\sigma$. For the simulations in the pore, the lateral box size is adjusted, depending on the concentration of the dipolar species, so as to keep a minimum number of dipoles around $N_2=100$. This corresponds typically to $N_1=5000$ hard spheres. When the dipoles become the majority species in the pore, the box size is reduced for saving time. Thus, the lateral box size in the pore ranges from $L=50\sigma$ to 15σ, for $H=3\sigma$. In this last situation, the corresponding number of hard spheres is rather small, but we checked that when the pore surface is doubled, the average particle densities do not change significantly. With $x_2^b=0.02$, $\rho_b=0.51$, $E^*=5$, for example, we find $\bar{\rho}_1=0.0216$ for $L=15\sigma$ to be compared to $\bar{\rho}_1=0.0215$ for $L=20\sigma$.

2. Treatment of the dipolar interaction

The treatment of the long-range contributions to the potential energy is a well known difficulty in the simulation of dipolar systems. For permanent dipoles, these contributions are in the dipole-dipole contribution U_{Dip}^{ij}

$$U_{\mathrm{Dip}}^{ij}=\frac{\boldsymbol{\mu}_{\mathrm{i}}\cdot\boldsymbol{\mu}_{\mathrm{j}}}{r_{\mathrm{ij}}^3}-3\frac{(\boldsymbol{\mu}_{\mathrm{i}}\cdot\boldsymbol{r}_{\mathrm{ij}})(\boldsymbol{\mu}_{\mathrm{j}}\cdot\boldsymbol{r}_{\mathrm{ij}})}{r_{\mathrm{ij}}^5}. \quad (1)$$

For bulk systems with periodic conditions in three directions, the total dipole-dipole potential energy is usually treated by the three-dimensional (3D)-Ewald summation method (see [29] for implementation details). In slab geometry, adapted 3D-Ewald summation techniques [26,30–32] are usually used. As in our previous work, to treat this long-range dipolar interactions [Eq. (1)], we used the simple version proposed by Yeh and Berkovitz [30]: a simulation box of dimensions L_x, L_y, L_z is used in which a vacuum region is incorporated in the z direction such as $L_z=H+L_{\mathrm{vacuum}}=\gamma L$ where L is the lateral dimension: $L_x=L_y=L$. Our implementation of this modified 3D-Ewald summation is similar to that detailed in the paper by Klapp and Schoen [26]). In Ref. [14], we made comparisons with their results to check the correctness of our implementation of the 3D-Ewald summation. In our recent work on induced dipoles [33] (see below),

we made further comparisons with the exact results for dipoles on a lattice. We took for the Ewald summation the set of parameters: $\alpha=7/L$, $\gamma=10$ that gives a gap width $\gamma L-H$ and $n^2=80$ for the terms in reciprocal space. As with permanent dipoles, no significant deviation was found between the exact electrostatic energy for a cubic lattice of permanent dipoles and the one obtained with these Ewald parameters and gap width. We moreover tested the impact of a variation of γ in situations where the pore is filled with the dipolar species and this for two pore widths $H=3\sigma$ and $H=9\sigma$. The results shown below were obtained with $\gamma=10$. Although such a large gap might be unnecessary in view of the possibility to use the electrostatic layer correction (ELC) [31,32] we kept it here since our objective was to test the physical ideas rather than to propose an optimized algorithm.

As detailed in [33], the specific situation of induced dipole raises the question of the time needed to compute the induced dipoles, in addition to the usual difficulty caused by the long-range dipolar interaction. This is especially true in slab geometry, since the standard reaction field method cannot be used then. In this work, we have shown that it is possible to combine the slab adapted 3D-Ewald summation with the appropriate treatment of the local field to efficiently treat induced dipoles confined in slab geometry. The main difficulty is then the computation of the induced dipoles, for a set $\{\boldsymbol{r}_i\}$ of particles coordinates sampled by the simulation algorithm. The $\{\boldsymbol{\mu}_\mathrm{i}\}$ are formally given by the system of equations,

$$\boldsymbol{\mu}_\mathrm{i} = \alpha_p \left(\boldsymbol{E}^{\mathrm{ext}} + \sum_{\substack{j \\ j\neq i}} \boldsymbol{T}_{ij} \cdot \boldsymbol{\mu}_\mathrm{j} \right), \tag{2}$$

where

$$\boldsymbol{T}_{ij} = \frac{1}{r_{ij}^3} \left(\frac{3\boldsymbol{r}_{ij}\boldsymbol{r}_{ij}}{r_{ij}^2} - \boldsymbol{I} \right) \tag{3}$$

and $\boldsymbol{I}$ is the identity matrix. Since the direct solution of Eq. (2) is impractical [34], it is more convenient to compute the local field $\boldsymbol{E}^{\mathrm{ext}} + \sum_{\substack{j \\ j\neq i}} \boldsymbol{T}_{ij} \cdot \boldsymbol{\mu}_\mathrm{j}$ by an iterative scheme. The one we have proposed for the specific case of the slab geometry is detailed in Ref. [33]. Once the $\{\boldsymbol{\mu}_\mathrm{i}\}$ are known, the potential energy is computed as

$$U(\{\boldsymbol{r}_i\}) = -\frac{1}{2} \sum_i \boldsymbol{\mu}_\mathrm{i} \cdot \boldsymbol{E}^{\mathrm{ext}}. \tag{4}$$

Note that since $U(\{\boldsymbol{r}_i\})$ depends only on the particles coordinates, the simulation steps do not involve the orientational moves required for permanent dipoles.

III. RESULTS, DISCUSSION

A. Nonadditive hard spheres: the PINBI effect

As recalled in the introduction, the proposed method for controlling the state of the adsorbed fluid takes advantage of the large variations in composition that occur in the confined fluid when the mixture with which it is in equilibrium in near the demixing instability. The simplest one is the mixture of nonadditive hard spheres in which the diameter is $\sigma_{ij}=\frac{1}{2}(\sigma_i+\sigma_j)(1+\delta)$ with $\delta>0$. The previous studies of refs [11,12] have shown that when the pore is in equilibrium with a mixture having a tendency to demix and which is highly asymmetric in composition—say $x_2^b=0.02$ for a non additivity parameter $\delta=0.2$—a population inversion occurs in the pore when the total bulk density ρ_b is varied: a jump in the adsorption of the minority species occurs after reaching a threshold value close to the coexistence density ρ_b^{coex}, and vice versa for the majority species. The population of the pore by the different species becomes the inverse of that of the bulk. This effect was thus referred to [11,12] simply as the population inversion (PI). To emphasize the importance of the closeness to the bulk instability, we found it better to designate it as the PINBI effect. In Ref. [11], the PI was found to be akin to capillary condensation of one-component fluids. An interpretation in terms of chemical potential and entropy was proposed. In the next section, we compare the phase diagrams of the nonadditive hard-spheres mixture in the bulk and in the pore to gain a better insight on this PINBI effect.

1. NAHS mixture: Phase diagram in the bulk and in the pore

Before presenting the results for the NAHS mixture we are interested in here, it should be recalled that the general phase diagram of binary mixtures can be quite complex, even in the simplest case with symmetric interactions—see for instance [35] and [36–38] for explicit calculations on model systems. These calculations show that the diagrams simplify somehow at high temperature, with a progressive reduction of the domain corresponding to the evaporation-condensation transition in comparison with that of the demixing one. In the limit of pure hard-core interactions (or infinite T) only the latter should survive, in accordance with the behavior expected for symmetric athermal mixtures. The general consequences of the symmetry on the fluid-fluid demixing of the NAHS mixture are summarized by Gazzillo (appendix of Ref. [39]) but in practice, the different approximate theories differ quantitatively. We thus consider here the phase diagram obtained from simulation. As illustrated for example in Refs. [18,40], the phase diagram of a symmetric mixture is most conveniently obtained by using the semigrand ensemble, with particle identity exchange [41]. The phase diagram of the confined and unconfined NAHS mixture (for the latter situation see also [42,43]) we obtained in this way for a nonadditivity $\delta=0.2$ is shown in Fig. 2.

To understand the connection between the bulk phase transition (here the fluid-fluid demixing) and the PINBI effect, we follow the analysis of the chemical potentials made in Ref. [35] for a symmetric AB mixture of Lennard-Jones particles, with strengths $\epsilon_{AB}<\epsilon_{AA}=\epsilon_{BB}$ (see the discussion of Fig. 2 [35]). This lower attraction between unlike-spheres favors demixing, as does the nonadditivity in HS mixtures with $\delta>0$. For such symmetric mixtures, one essential point is the symmetry of the phase separation curves in the concentration-total density plane (x_2,ρ_b), with respect to $x_2=0.5$. Upon increasing the density at constant $x_2<0.5$ (species 2 is the minority species), we have for the chemical

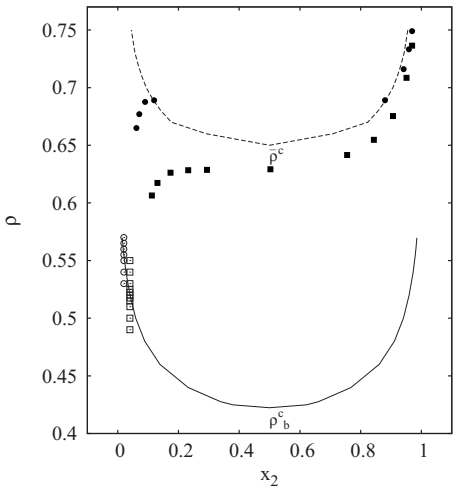

FIG. 2. Phase diagram (demixing) of the nonadditive hard-sphere mixture with nonadditivity parameter $\delta=0.2$, in the bulk (full curve) and in a pore of width $H=3\sigma$ (dotted curve). The filled symbols show the $\rho-\bar{x}_2$ trajectory in the phase diagram corresponding to Figs. 4 and 5 for a pore in equilibrium with a bulk mixture with composition $x_2^b=0.04$ (squares) and $x_2^b=0.02$ (circles). The empty symbols show the corresponding series of bulk densities at fixed x_2^b.

potentials the sequence $\mu_2<\mu_1$ before the demixing transition, $\mu_2=\mu_1$ on the coexistence boundary ($\rho_b=\rho_b^{coex}(x_2)$) and $\mu_2>\mu_1$ inside the two-phase demixed region. The reason for this sequence is the increasing role of the binding energy in comparison with the entropy of mixing as the density increases [35]. In the NAHS mixture, the role of the binding energy is played by the packing effect, embodied in the excess chemical potential μ_i^{ex} defined by $\beta\mu_i=\ln\rho\Lambda_i^3+\ln(x_i)+\beta\mu_i^{ex}$ (with Λ_i the thermal wavelength of component i). The increase of the excess chemical potential of the majority species (easier to insert due to the nonadditivity) eventually offsets the difference due to the ideal gas contribution $\ln x_i$. In the symmetric region $x_2>0.5$, the sequence is the reverse one: $\mu_2>\mu_1$ before phase separation, $\mu_2=\mu_1$ on the coexistence line and $\mu_2<\mu_1$ inside the two-phase region (see Fig. 3). Therefore, the equality of the chemical potentials occurs on the line $x_2=0.5$, below the critical density ρ_b^c and on the coexistence line for $\rho_b>\rho_b^c$. Now, as shown in Fig. 2, the phase diagram in the pore is of course also symmetrical, the key point being the stabilizing role of the confinement against demixing: the critical density is then higher $\bar{\rho}^c>\rho_b^c$ (see also Fig. 1 in [18]). In the concentration-density plane, there thus exists a region $\rho_b^c<\rho<\bar{\rho}^c$ in which the order of the chemical potentials in the bulk ($\mu_2>\mu_1$ for $x_2<0.5$) is the opposite of that in the pore ($\mu_2<\mu_1$). Recalling that the pore/bulk equilibrium requires the equality of the chemical potentials for each component in the bulk and in the pore, the only possibility for having at the same density $\mu_2(\bar{x}_2)>\mu_1(\bar{x}_2)$ (in the pore) while $\mu_2(x_2)>\mu_1(x_2)$ (in the bulk) is to have $\bar{x}_2>0.5$. Since we assumed $x_2<0.5$, this means that the minority species in the bulk becomes the majority one right after passing the bulk demixing boundary. One may then anticipate that an increase of the bulk density ρ_b at fixed composition $x_2<0.5$ goes with a similar one of the density $\bar{\rho}$

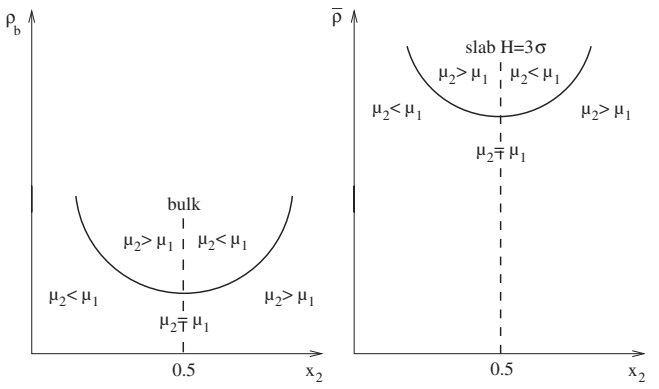

FIG. 3. Theoretical chemical potentials sequence in the NAHS mixture and demixing lines in the bulk (left panel) and in confinement (right panel). The equality $\mu_1=\mu_2$ occurs either on the coexistence line or on the equal composition one, $x_2^b=0.5$.

in the pore, first with an average mole fraction $\bar{x}_2\approx x_2$. When ones reaches the bulk boundary $\rho_b^{coex}(x_2)$, the chemical potentials $\mu_1(x_2)$ and $\mu_2(x_2)$ become equal, with $\mu_2=\mu_1$ also in the pore. If the associated average density $\bar{\rho}$ is lower than $\bar{\rho}^c$, the critical density in the pore, the equality $\mu_2=\mu_1$ in the pore requires that the average concentrations be also equal, $\bar{x}_1=\bar{x}_2=0.5$. After the value $\bar{x}_2=0.5$, the minority species (in the bulk) becomes the majority one in the pore. In that case, the population inversion in the pore is progressive, as shown by the black squares in Fig. 2, for $x_2^b=0.04$. For the lower concentration $x_2^b=0.02$, shown by black circles, equal chemical potentials in the bulk and in the pore requires a higher average density in the pore (recall that the coexistence curve for which the chemical potential become equal is shifted upward). $\bar{\rho}$ can then be above the critical density $\bar{\rho}^c$. Upon increasing ρ_b, the demixing boundary is then reached both in the bulk and in the pore. A slight increase of ρ_b will thus lead to a demixed mixture, the phase poor in the species 2 coexisting with the symmetric one. For the highly asymmetric overall compositions considered here, the demixed mixture will however consist mostly of the phase whose composition is closest to the overall one (for the properties we are interested in, only the global composition is truly relevant). In a grand-canonical simulation with $\mu_2\neq\mu_1$, one may also simulate metastable homogeneous states beyond the actual stability limit, due to limited spontaneous transitions [44]. This might occur when one crosses the coexistence domain, as shown by the black circles ($x_2^b=0.02$) illustrating a sudden change in population from $\bar{x}_2\approx x_2^b$ to $\bar{x}_2\approx x_1^b=1-x_2^b$. Therefore, with an *overall* composition $x_2^b\ll 0.5$, the mean bulk composition will in any case (metastable *and* demixed states) differ widely from that in the pore, in the vicinity of the bulk instability. The corresponding adsorption curves are shown below.

2. Density driven PINBI

In Figs. 4 and 5, we show the population inversion curves for a nonadditive HS mixture with $\delta=0.2$ and a pore width $H=3$, for $x_2^b=0.04$ and $x_2^b=0.02$. In the former case, we observe the progressive inversion we have just discussed. We

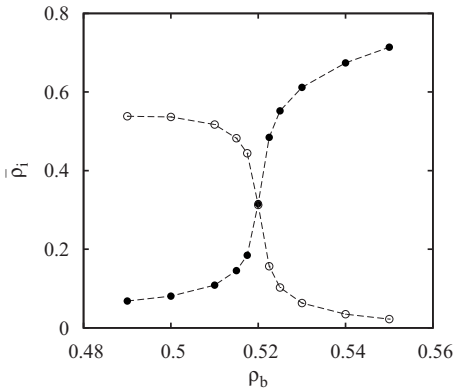

FIG. 4. Average densities in the confined NAHS mixture as a function of the bulk density at fixed bulk concentration $x_2^b=0.04$. The filled circles correspond to the adsorption of the minority species in a pore of width $H=3\sigma$ and the empty circles to the desorption of the majority one. The lines are guides to the eyes.

immediately check that the adsorption and desorption curves precisely cross for the bulk density $\rho_b^{coex}(x_2^b=0.04)$ of Fig. 2. For the smaller concentration, the adsorption is more abrupt, the jump occurring for $\rho_b \approx 0.555$, slightly inside the bulk demixed phase [the density at the jump is more evident than in Fig. 2(a) of [2] due to a more accurate analysis of the concentration histograms, as in Fig. 6].

In Ref. [11], Jiménez-Angeles *et al.* found that the inversion line is close to the bulk fluid coexistence line but the two phenomena are different. They stated that the PI occurs before the bulk coexistence as ρ_b increases at fixed x_2^b. They however did not define precisely the threshold density for the PI. If one takes as a criterion the condition in which the average concentration becomes much larger than the bulk one, say $\bar{x}_2 \approx 10x_2^b$, one might indeed consider that the PI starts before the bulk instability. A criterion for a strict inversion $\bar{x}_2 > x_1 > 0.5$ would however require crossing the bulk demixing line. From the consideration of the chemical potentials of the NAHS mixture, this density driven PINBI seems actually directly connected with the bulk demixing instability, through the sequence of chemical potentials. When it is gradual, it is so because the mixture remains homogenous, being stabilized in the pore by confinement. When it is abrupt, it is related either to the demixing also in the pore or

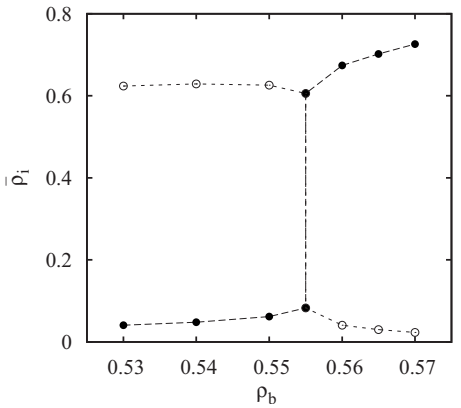

FIG. 5. Same as Fig. 4, for $x_2^b=0.02$.

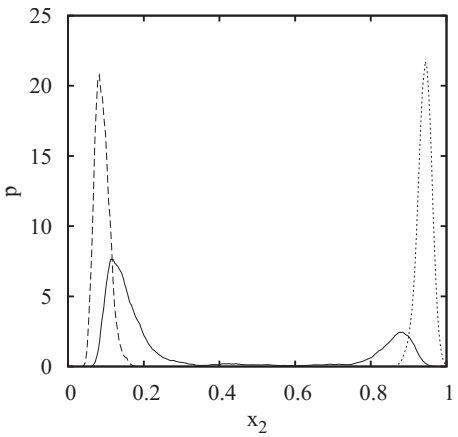

FIG. 6. Concentration Histograms of species 2 in the pore, at fixed bulk concentration $x_2^b=0.02$ and bulk densities $\rho_b=0.550$ (dashes), 0.555 (lines), and 0.560 (dots). For $\rho_b=0.555$, a mixture poor in species 2 ($\bar{x}_2 \approx 0.12$) coexists with a concentrated one ($\bar{x}_2 \approx 0.88$).

possibly to metastable states and hysteretic behavior. As shown in Fig. 6, there is a brief incursion in the pore demixed phase upon varying the density about $\rho_b^{coex}(x_2^b=0.02)$, the overall effect being always a sudden jump in the adsorption of the bulk minority species when crossing the bulk demixing boundary (see below the case $H=9\sigma$ in which stabilization by confinement is less efficient than for $H=3\sigma$). Regardless of this, the essential point is then that the density in the liquidlike phase should be close to the value after the adsorption jump (see [44] for a similar discussion for one-component systems). We will not discuss here further these observations (for related phenomena, see for, e.g., [44–46] and [47,48] for reviews) since an important mechanism in the presence of dipoles is the coupling with the applied field, a situation we will examine in the next section.

To anticipate this, we show in Fig. 7 the density induced PINBI when one species bears a permanent dipole. For the value of the dipole moment considered here, there is no essential difference with the pure NAHS mixture: for the same

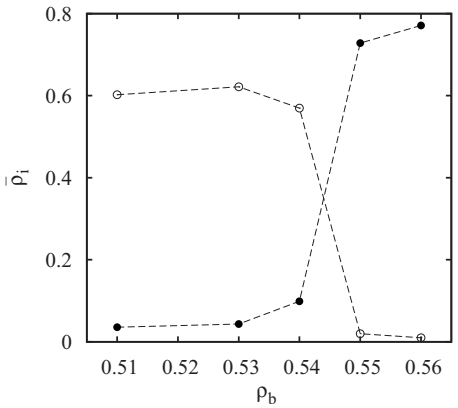

FIG. 7. Average densities in the confined nonadditive mixture of hard spheres and dipolar hard spheres of equal diameter σ and $\delta=0.2$ as a function of the bulk density at fixed bulk concentration $x_2^b=0.02$, pore width $H=3\sigma$ and $\mu^*=1$; *filled circles:* adsorption of the dipolar hard spheres. The lines are guides to the eyes.

hard-core nonadditivity parameter $\delta=0.2$ and $x_2^b=0.02$, the population inversion occurs for $\rho_b=0.555$ for a pure nonadditive HS mixture and between 0.54 and 0.55 for the hard-sphere dipole mixture with $\mu^*=1$ and $H=3\sigma$. A relatively small μ^* was taken precisely for not departing too much from the conditions in which the PINBI in the NAHS mixture occurs. However, the analysis made above from the sequences for the chemical potentials cannot be transposed directly to the mixture of hard-spheres and dipolar hard-spheres since the particles no longer play a symmetric role. The trend related to the increased free volume in the pore [11] is consistent with a preferred orientation of the dipoles parallel to the walls, but the competition of the parallel and head to tail configurations of the dipoles which contribute by a different sign to the electrostatic energy complicates the analysis. It is also clear that the presence of dipolar interactions complicates even further the general phase diagram of the mixture. Even in the bulk phase, the study of the phase diagram of mixtures comprising dipolar species remains still challenging (see for instance Refs. [49–54]). According to the different estimates made in these studies, a mixture of hard-spheres and dipolar hard-spheres with *additive* diameters and $\mu^*=1$ should remain in a homogeneous state in the range of bulk densities considered below $\rho_b \approx 0.5-0.56$. The case of nonadditive diameters has not been considered before and we made not attempt to determine the phase diagram in this case (the stability of some state points in the vicinity of the threshold density has been checked by studying the system size dependence of concentration histograms in the grand-canonical simulation). An indication was given above that the bulk instability indeed plays an important role also when one of the species is dipolar (compare Figs. 5 and 7). This qualitative observation will be confirmed in the last section by comparing the effect of the field on the filling by mixtures of hard spheres and dipolar hard spheres, in the additive and nonadditive cases. This is why a reference to the closeness to the bulk instability should also be appropriate when discussing the population inversion in mixtures comprising dipolar particles.

B. Mixture of hard-spheres and dipolar hard-spheres in an external field: The field induced PINBI effect

The previous section has shown that strong variations in the composition of the adsorbed fluid can take place when the state of the bulk fluid is close to the demixing boundary. One then anticipates that a tiny perturbation about this might trigger these variations. This is the idea behind the field induced population inversion (F-PINBI) effect. To better distinguish the two basic mechanisms that contribute to this F-PINBI we discuss in the next section an external field driven adsorption of a pure dipolar fluid.

1. Field-induced adsorption of dipolar particles

This second basic mechanism—field induced pore filling by a one-component dipolar fluid is shown in Fig. 8. At increasing field strength E^*, the pore is progressively filled by the dipoles. The filling rate depends on ρ_b, E^*, and μ^* and the field direction. For the value used here, the explanation

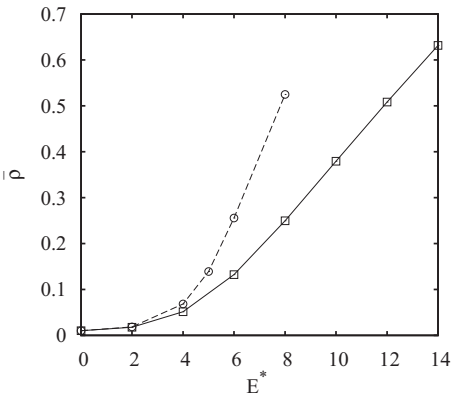

FIG. 8. Effect of the field direction on the field induced filling of a pore by a one-component dipolar fluid for $\mu^*=1$ and $H=3\sigma$. The pore is in equilibrium with a bulk fluid with density $\rho_b=0.0102$. The field is not applied in the bulk. Circles: parallel field. Squares: normal field. The lines are guides to the eyes.

seems that the field-dipole interaction energy $-\Sigma_i \boldsymbol{\mu}_i.\boldsymbol{E}$ offsets the entropy loss due to their orientation in the direction of the field. This explanation is corroborated by the effect of changing the field direction, the dipoles being more efficiently adsorbed in a parallel field configuration. This is understandable from the formation of head-to-tail dipolar chains oriented preferentially in the direction of the field. These chains, *a priori* with arbitrary length, favor a much greater decrease in electrostatic energy than in the normal field configuration. In the latter case, indeed, the maximum chain length is imposed by the number of dipoles layers that can fit in the pore, depending on its width (here 3 for $H=3\sigma$). This external field induced pore filling has of course been demonstrated in previous studies—see for example [20,21] for water in nanopores, in particular Fig. 1 in the last reference. Note that the equilibrium state in presence of the field may not always be the filled one at other parameters or if more complex interactions are considered (see Ref. [20] for example), due to the competition between energetic and entropic contributions.

2. Field-induced PINBI

The previous sections have shown the two basic mechanisms acting separately: strong variations in composition near the bulk instability and field promoted adsorption of dipolar species. We may now combine them to produce the desired effect. To this end, we first need a bulk fluid state (ρ_b, x_2^b) that favors the population inversion in the pore, without field, say (0.55,0.02) for $H=3\sigma$, $\delta=0.2$, and $\mu^*=1$ (the results shown in this section have been obtained with these values). We next apply the external field, only in the pore region. The latter will thus act as a potential energy sink for the dipolar particles. For the two mechanisms to combine in the desired direction, the dipolar species must be the minority one in the bulk. We then anticipate that the closer we are from the threshold density without field, the weaker will be the external field E_{tr}^* required to trigger it. This is shown for $x_2=0.02$ in Fig. 9. In the most favorable case ($E^*=0.5$), the actual value of E_{tr} is about $3\ 10^{-3}$ V/μm for $T=300$ K,

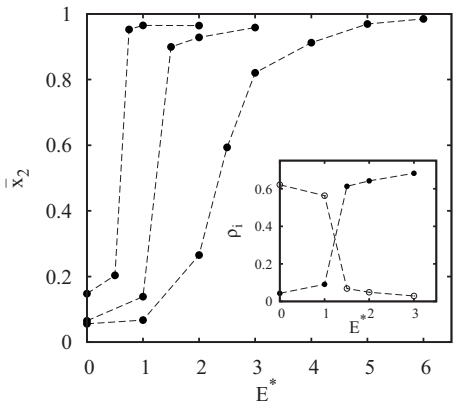

FIG. 9. Dipoles mole fraction in the pore as a function of the reduced applied field strength. The pore is in equilibrium with a bulk fluid with $x_2^b=0.02$ and total densities (from right to left) $\rho_b=0.51,0.53,0.54$. The inset shows the corresponding dipoles and hard-spheres density in the pore for $\rho_b=0.53$. Lines are guides to the eyes.

$\sigma=1$ μm and $\mu=2\times10^5 D$. A small variation of the applied field produces the inversion: the dipolar particles are selectively absorbed by a weak change about E_{tr}, the converse being also possible.

To be convinced that this is a real change in composition induced by the applied field, one just has to compare the situation for $\rho_b=0.51$ and 0.53 at zero field (Fig. 7) with the corresponding one in the presence of the field. In the former case, the average composition $\bar{x}_2$ in the pore is close to the bulk overall composition $x_2^b=0.02$, for both densities. Even if the bulk were in a phase separated state, the pore composition after the jump is widely different from the mean one in the bulk, dominated by the phase whose composition is closest to the overall one, as recalled above. Since the field is next applied only in the pore—and hence at fixed bulk state—the observed sudden change in the pore composition $\bar{x}_2$ is thus certainly a true change in population. To better ascertain the bulk state, we nevertheless checked that for $\rho_b=0.51$, the bulk concentration histograms obtained from a GC simulation using the chemical potentials obtained from the canonical simulation become more and more peaked about $x_2^b=0.02$, as the box size increases, independently of the initial configuration. This confirms that this is a stable state. For $\rho_b=0.53$, closer to the threshold density, the same trend was found when starting from a configuration with few dipoles (hence close to the overall composition) but the study of the box size dependence is limited by the computer time required when starting from a configuration representative of the symmetric phase ($x_2\approx0.98$), that involves a large number of dipoles. We may nevertheless state that a field induced population inversion certainly exists in the range of densities shown in Fig. 9.

The density profiles reflect of course these large variations in the composition that occur at the adsorption jump, as shown in Fig. 10. Note that in order to have a significant number of dipoles in the pore before the inversion, a larger box is used as discussed in section *B*.1. For a larger concentration $x_2=0.04$, the behavior is qualitatively similar (Fig. 11) for $\rho_b=0.49$, but the variation of the adsorption curve is more progressive, as for the pure NAHS mixture at the same concentration (see Fig. 2). We tentatively included the data for a higher value $\rho_b=0.50$. The average concentration in the pore is then difficult to obtain due to large statistical fluctuations, possibly because the bulk is then close to the critical point. Further simulations are necessary to clarify the behavior in these conditions.

Since the combination of these two generic mechanisms provides in principle a very sensitive and flexible control of the pore filling, it is important before proceeding further to see if the relevant physical parameters are realistic. In the context of colloids, we first note that for a particle diameter of 1 μm and $T=300$ K, for example, a value $E^*=8$ (beyond which the slope of the adsorption curve in figure becomes constant) corresponds to $E=49\times10^{-3}$ V/μm and $\mu=2\times10^5 D$—see also Sec. D in Ref. [14] for a more detailed discussion of the relation with the parameters of real systems. We will also show below that the required magnitude of the dipole moment can be obtained with reasonable value of the polarizability of the material forming the dipolar particles. A permanent dipole is hence not a necessary condition. Considering now molecular systems, the same value of μ^* is also appropriate for the dipolar interaction between *molecular* species, thanks to the scaling factor $\sigma^{-3/2}$ in its definition. The dipole moment being then of the order of one Debye, a field strength of the order 10 V/nm is needed to obtain the same reduced energy $-\mu^* E^*$. Such field strengths are not unusual for confinement at the molecular scale. Although the basic parameters seem thus realistic also in this regime, the remaining question is then the role of specific interactions not considered in the present simple model, say a preferential adsorption potential for the more polar molecule. A greater

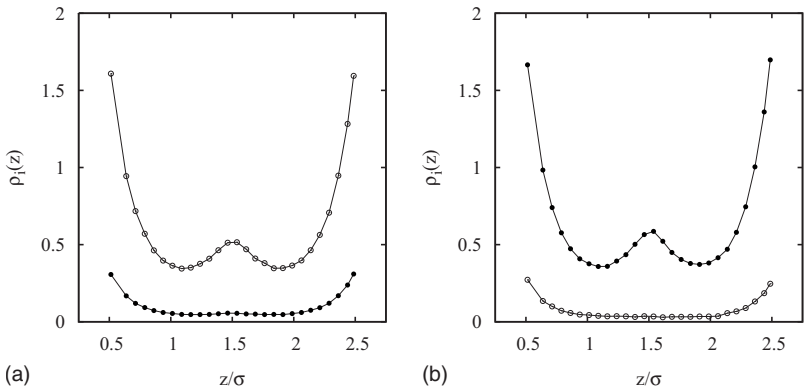

FIG. 10. Density profiles in a nonadditive mixture of dipolar hard spheres (*filled circles*) and hard spheres (*open circles*), before (a) and after (b) the population inversion. The pore is in equilibrium with a bulk fluid at $\rho_b=0.53$ and $x_2^b=0.02$. Some data points have been removed for clarity

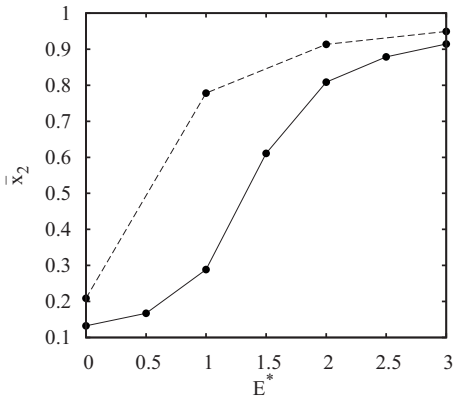

FIG. 11. Dipoles mole fraction in the pore as a function of the reduced applied field strength. The pore is in equilibrium with a bulk fluid with $x_2^b=0.04$ and total densities (from right to left) $\rho_b=0.49$ (right) and 0.50 (left). Lines are guides to the eyes.

diversity of scenarios becomes then possible (similar ones for colloids are given in our previous work [14]). With this reservation, we may safely discuss below the role of the other, less critical, parameters (at least in this minimal model).

3. Role of the different parameters

(a) F-PINBI in parallel field. The role of the direction of the field has been shown above (Fig. 8) in the case of a one-component dipolar fluid. Figure 12 below for a mixture of hard spheres and dipolar hard spheres compares the two field directions. It confirms a more efficient F-PINBI effect in parallel field. This is in line with the discussion of the potential energy decrease by long chains parallel to the walls. From a practical point of view, however, a normal field configuration with the pore walls acting as the plates of a "parallel capacitor" as in Ref. [3] is achieved rather easily whereas the $E_\parallel$ one would entail finite size effects, inhomogeneity of the field etc., that might complicate the design of practical devices.

(b) Role of the pore width. One important parameter in this geometry is the pore width. It determines in particular the maximum number of layers that can fit in the pore. Quite generally, the stabilizing effect of the pore is less efficient as the pore width increases, since one approaches then the bulk behavior. The adsorption curves for $H=3\sigma$ and $H=9\sigma$ are compared in Fig. 13. The greater steepness of the adsorption curve for the larger pore seems indeed coherent with a greater proximity to the demixing boundary. Having two phases in equilibrium in the pore might constitute a limitation if the desired effect is to have a stronger contrast in the physical response between the empty and filled states by the bulk minority species. This inconvenience might accordingly offset the advantage of a larger pore width, more easily achieved in practice. The extent of the two-phase domain needs confirmation by a full mapping of the pore-pore and pore-bulk phase diagram as a function of the pore width, a rather lengthy task that requires the response for a specific system to be undertaken. The possibility of having two coexisting phases is illustrated in Fig. 14 in a pore with $H=9\sigma$ and a parallel field. Note that the chemical potentials are here fixed, the coexisting phases for a given field strength being obtained by starting from different initial conditions. No spontaneous transition is however found between the two

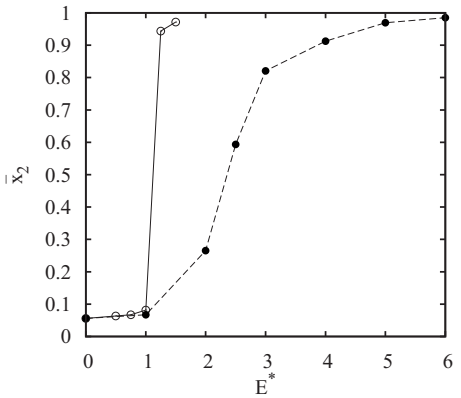

FIG. 12. Effect of the field direction on the F-PINBI in a pore with $H=3\sigma$. The pore is in equilibrium with a bulk fluid at fixed density $\rho_b=0.51$ and $x_2^b=0.02$. *Empty circles:* parallel field, *filled circles:* normal field.

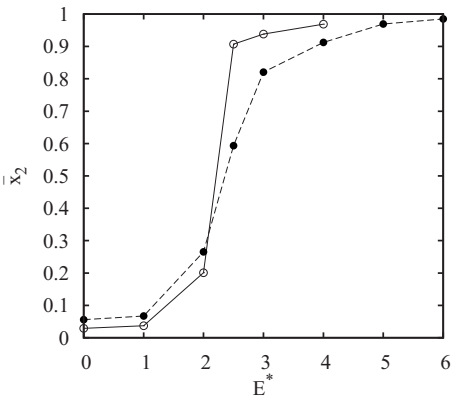

FIG. 13. Effect of the width of the pore on the F-PINBI with normal field. *Filled circles:* $H=3\sigma$, *empty circles:* $H=9\sigma$. The pore is in equilibrium with a bulk fluid with density $\rho_b=0.51$ and $x_2^b=0.02$.

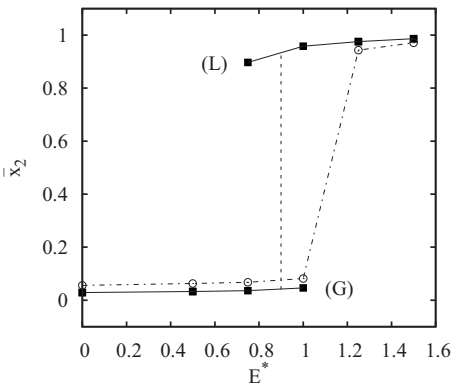

FIG. 14. Effect of the width of the pore on the field induced PINBI with parallel field. *Filled squares:* $H=9\sigma$, *empty circles:* $H=3\sigma$. In the pore with $H=9\sigma$, a liquid (l) phase coexists with a gaz (g) phase of dipoles around the adsorption jump ($E^*\approx 1$).

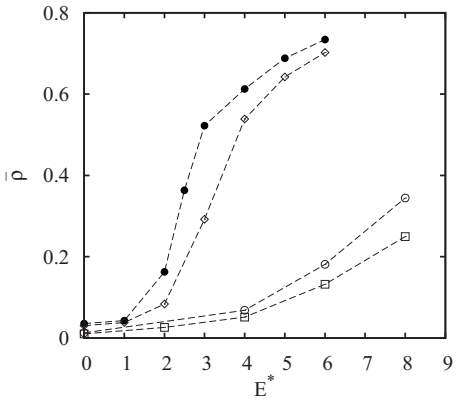

FIG. 15. Effect of the applied field on the filling of the pore by different model fluids. $\bar{\rho}$ is the density of the dipolar species, in the pore ($H=3\sigma$). *Empty squares*: one-component dipolar fluid [for $\rho_b=0.0102$ as in Fig. 8; *open circles*: additive mixture of hard spheres and dipoles (with $x_2=0.02$ and $\rho_b=0.51$ in the bulk)]. *Diamonds*: same for a Yukawa repulsion between the dipoles and the hard spheres; *filled circles*: same for the nonadditive hard spheres—dipolar hard-spheres mixture. The range of the Yukawa potential (with $\epsilon*=8$) gives the same contribution to the second virial coefficient as the nonadditive hard-spheres potential with $\delta=0.2$.

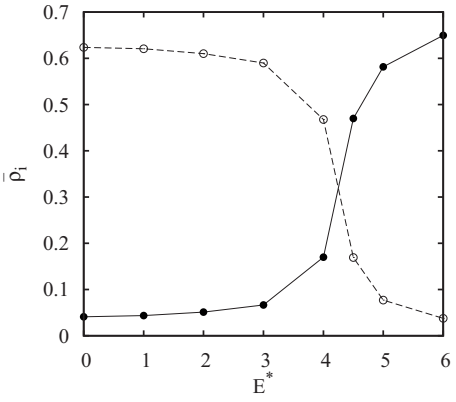

FIG. 16. Electric field controlled population inversion for a nonadditive mixture of hard-spheres and polarizable hard-spheres in a pore with $H=3\sigma$. The total reservoir density is $\rho_b=0.53$. The bulk mole fraction of the polarizable hard spheres is $x_2=0.02$. ρ_i: density of each species; E^*: applied field strength. *Filled circles*: polarizable hard-spheres, *Open circles*: hard spheres. Lines are a guide to the eyes.

phases as for example in Fig. 6 because of the large free energy separation between these phases. The question of the metastability of such confined phases obtained from a grand-canonical simulation should however be considered again [44] (see also [55]), but the main effect—field induced adsorption jump—is unaffected. The curve for $H=3\sigma$ also shown illustrates the other scenario in which a jump in adsorption occurs without having two coexisting phases, confirming again the stabilizing role of confinement. As regards the confinement geometry, we notice that for the pure NAHS mixture, the threshold density for a cylindrical pore [11] of radius $R=3.5\sigma$ is quite similar for $x_2=0.02$ to the one we find here in slab geometry with $H=3\sigma$, without field ($\rho_b \approx 0.555$). The fact that we find a more gradual PI for $x_2=0.04$ suggests that the confinement is "weaker" in the cylinder of radius 3.5σ than in the slab of width 3σ. The threshold density ($\rho_b \approx 0.52$) is again very similar in the two geometries, confirming the role of the bulk phase separation, through the equality of the chemical potentials.

(c) Other parameters. As a first check of the sensitivity of the conclusions to some other aspects of the model, we first considered the effect of a different interaction u_{12} between species 1 and 2. The tendency to demix in the bulk is indeed a necessary condition for having a steep population inversion curve. That this F-PINBI phenomenon is quite general and not a lucky outcome of the nonadditive hard sphere potential is illustrated in Fig. 15: a Yukawa repulsive potential having a range of the order of the nonadditivity of the NAHS and same contribution to the second virial coefficient gives a very similar adsorption curve, whereas the pattern followed by a mixture of pure hard spheres and dipolar ones with additive hard-core diameters is very similar to the one for the pure dipolar fluid. The requirement for observing a sensitive field effect is that the self-coordination should be more favored in the mixture. With colloids, the poor miscibility can be favored by suitable chemical composition of the particles surface layers (see for, e.g., [56,57]), the same being true for the absence of specific interaction with the pore walls, covered say with polymer brushes (see for example [19] and [58] and refs. therein for recent experimental work).

As recalled in the introduction, for this method to be as generic as possible, with simple ingredients it is desirable that this F-PINBI should also be observed with polarizable (macro) particles rather with ones bearing a permanent dipoles such as ferrocolloids. We thus considered a mixture of hard spheres and polarizable hard spheres with nonadditive diameters. For the latter, we took a polarizability $\alpha_p=0.04\sigma^3$ (in order to model colloidal particles). The mixture with nonadditivity parameter $\delta=0.2$ is confined in a pore of width $H=3\sigma$. Since the electric field is applied only in the pore, the bulk fluid that fixes the chemical potentials is the same mixture of nonadditive hard spheres, but without polarization. To remain close to the conditions of the PINBI for permanent dipoles, we again took a total reservoir density $\rho_b=0.53$ and a bulk mole fraction of the polarizable particles $x_2^b=0.02$. In Fig. 16, we show the population inversion in the pore for the polarizable particles. The technical details of the treatment of polarizable particles in slab geometry are detailed in our previous work [33] (see also [59]). The inversion is still present but it occurs for a field that is four times stronger than for permanent dipole [2]. These results depend of course on the value of α_p and the comparison with permanent dipole is not immediate, since the dipole moment changes with the applied field. Even so, the threshold field strength remains relatively small. This shows that polarizable colloids are quite generic candidates for the observation of this F-PINBI effect. Polarizable colloidal particles are actually rather common, since polarizability of the materials forming the colloids, say the electronic one, is always present to some extent. Examples are polymethylmethacrylate (PMMA) [60] or polystyrene Latex particles [61]. Polarizability is also quite frequent in core-shell nanoparticles [62].

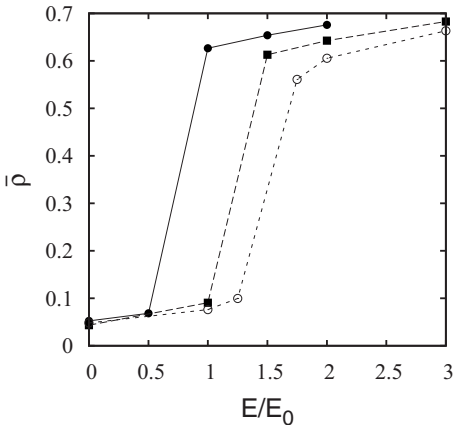

FIG. 17. Adsorption-field strength curves at different temperatures. The symbols show the dipoles mean density in the pore at $T=285$ K, 300 K and 325 K from left to right. The bulk mole fraction is $x_2=0.02$ and the total bulk density is $\rho_b=0.53$. Here $E/E_0=E^*(300)(T/300)^{1/2}$. The value of E_0 which fixes the field strength scale can be determined by specifying σ, with $T=300$ K

Finally we show in Fig. 17, the effect of a temperature change, an important practical parameter indeed. Notice that one cannot use the data for a given set of reduced variables E^* and μ^* to obtain directly the data at different temperatures at a given value of the actual field strength E and dipole moment μ, because the reduced variables combine both E and μ with T. Considering, for example, the data shown in Fig. 17 for $\mu^*=1$ as a function of E^* as corresponding to $T=300$ K with E and μ fixed (this corresponds to the medium curve in Fig. 9), one has to redetermine the new values of the reduced chemical potentials and field strengths at different T, by rescaling E^* by the factors $T^{-1/2}$. The simulation must thus be rerun both in the bulk and in the pore for each temperature and field strength. The result is shown in Fig. 17 for $T=300\pm25$ K. We observe that near the adsorption jump ($\rho_b=0.53$, $E^*=0.5$ for $\mu^*=1$) a slight change in temperature ($\delta T=25$ K in Fig. 17) produces a detectable change in adsorption, which may be important for some applications.

IV. CONCLUSION

In conclusion, the results presented in this work confirm that the combination of two quite generic mechanisms allows a flexible control of the adsorption of the different species in an open pore in equilibrium with a bulk mixture. In particular, the main observation—a field induced population inversion near the bulk demixing instability—has been shown to be a robust phenomenon, by considering the effect of the most influential parameters—bulk composition, field strength and direction, polarizability of the particles and pore width. This effect has been demonstrated from a minimal model for the interactions between the particles and between the latter and the confining medium. It should thus concern first the systems that are closest to these optimum conditions, say pseudobinary mixtures of hard-sphere-like colloids. In order to benefit from the field effect, one species should be either polar (e.g., ferrocolloid in magnetic fields) or much more polarizable than the other (the presence of a permanent dipoles being unnecessary). To conform to the simple conditions considered here, the solution should not contain free charges to avoid particle motion due to the action of the field (electrohydrodynamic flows). On the other hand, the basic mechanisms (demixing instability and coupling with an external field) exist also for some atomic or molecular mixtures adsorbed in nanopores. Since the dimensionless variables we used might correspond to the actual magnitude of the interactions in such conditions, this prediction should concern a broader class of systems than mesoscale ones. At such molecular scale, however, a great diversity of scenarios should emerge due to specific interactions. In this respect, it is also clear that even in the case of colloids, multiple scenarios might be possible by varying the different physical parameters—dipole moment strength, size asymmetry, nonadditivity, pore width, non uniform fields, etc. Only a small part of it has been considered in this work. We thus believe that the results presented here justify further experimental studies and simulations of the system considered here, given the diversity of possible applications of this field controlled composition of the confined fluid and hence flexible control of the physical properties that depend on the composition of the confined fluid. This varying composition is the key feature which distinguishes the method discussed here from previous ones aimed at a similar control of the state of the adsorbed fluid. As examples, we suggest to modulate in this way the dielectric response of the confined fluid for optical applications or its viscosity for electromechanical ones.

[1] *Fundamentals of adsorption: Proceedings of the Fourth International Conference on Fundamentals of Adsorption*, Kyoto, edited by M. Suzuki (Elsevier, Amsterdam, 1993).
[2] C. Brunet, J. G. Malherbe, and S. Amokrane, J. Chem. Phys. **131**, 221103 (2009).
[3] T. Gong and D. W. M. Marr, Langmuir **17**, 2301 (2001).
[4] T. Gong, D. T. Wu, and D. W. M. Marr, Langmuir **18**, 10064 (2002).
[5] T. Gong, D. T. Wu, and D. W. M. Marr, Langmuir **19**, 5967 (2003).
[6] C. Bechinger, Curr. Opin. Colloid Interface Sci. **7**, 204 (2002).
[7] Z. Tan and Keith E. Gubbins, J. Phys. Chem. **96**, 845 (1992).
[8] V. Lachet, A. Boutin, B. Tavitian, and A. H. Fuchs, Faraday Discuss. **106**, 307 (1997).
[9] F. K. Katsaros, Th. A. Steriotis, G. E. Romanos, M. Konstantakou, A. K. Stubos, and N. K. Kanellopoulos, Microporous Mesoporous Mater. **99**, 181 (2007); J. Pires, M. Bestilleiro, M. Pinto, and A. Gil, Sep. Purif. Technol. **61**, 161 (2008); A. Busch, Y. Gensterblum, B. M. Krooss, and N. Siemons, Int. J. Coal Geol. **66**, 53 (2006).
[10] A. Yethiraj and A. van Blaaderen, Nature (London) **421**, 513 (2003).

[11] F. Jiménez-Angeles, Y. Duda, G. Odriozola, and M. Lozada-Cassou, J. Phys. Chem. C **112**, 18028 (2008).
[12] S. Kim, S. Suh, and B. Seong, J. Korean Phys. Soc. **54**, 660 (2009).
[13] A. Z. Panagiotopoulos, Mol. Phys. **62**, 701 (1987).
[14] C. Brunet, J. G. Malherbe, and S. Amokrane, J. Chem. Phys. **130**, 134908 (2009).
[15] A. Ayadim, J. G. Malherbe, and S. Amokrane, J. Chem. Phys. **122**, 234908 (2005).
[16] S. Amokrane, A. Ayadim, and J. G. Malherbe, J. Phys. Chem. C **111**, 15982 (2007).
[17] L. Sarkisov and P. A. Monson, Langmuir **17**, 7600 (2001).
[18] Y. Duda, E. V. Vakarin, and J. Alejandre, J. Colloid Interface Sci. **258**, 10 (2003).
[19] A. De Virgiliis, R. L. C. Vink, J. Horbach, and K. Binder, Phys. Rev. E **78**, 041604 (2008).
[20] S. Vaitheeswaran, J. C. Rasaiah, and G. Hummer, J. Chem. Phys. **121**, 7955 (2004).
[21] D. Bratko, C. D. Daub, K. Leung, and A. Luzar, J. Am. Chem. Soc. **129**, 2504 (2007).
[22] H. Zou, S. Wu, Q. Ran, and J. Shen, J. Phys. Chem. C **112**, 11623 (2008).
[23] R. R. Kotdawala, N. Kazantzis, and R. W. Thompson, J. Chem. Phys. **123**, 244709 (2005).
[24] I. Szalai and S. Dietrich, Eur. Phys. J. E **28**, 347 (2009).
[25] S. H. Lee, J. C. Rasaiah, and J. B. Hubbard, J. Chem. Phys. **85**, 5232 (1986).
[26] S. H. L. Klapp and M. Schoen, J. Chem. Phys. **117**, 8050 (2002); J. Jordanovic and S. H. L. Klapp, Phys. Rev. Lett. **101**, 038302 (2008).
[27] J. Richardi, M. P. Pileni, and J.-J. Weis, J. Chem. Phys. **130**, 124515 (2009).
[28] A. V. Neimark and A. Vishnyakov, J. Chem. Phys. **122**, 234108 (2005).
[29] M. P. Allen and D. J. Tildesley, *Computer Simulation of Liquids* (Oxford Science Publication, New York, 1987).
[30] I.-C. Yeh and M. L. Berkowitz, J. Chem. Phys. **111**, 3155 (1999).
[31] A. Arnold, J. de Joannis, and C. Holm, J. Chem. Phys. **117**, 2496 (2002); J. de Joannis, A. Arnold, and C. Holm, *ibid.* **117**, 2503 (2002).
[32] A. Brodka, Chem. Phys. Lett. **400**, 62 (2004).
[33] C. Brunet, J. G. Malherbe, and S. Amokrane, Mol. Phys. (in press).
[34] F. J. Vesely, J. Comput. Phys. **24**, 361 (1977).
[35] O. Antonevych, F. Forstmann, and E. Diaz-Herrera, Phys. Rev. E **65**, 061504 (2002).
[36] D. Pini, M. Tau, A. Parola, and L. Reatto, Phys. Rev. E **67**, 046116 (2003).
[37] R. Fantoni, D. Gazzillo, and A. Giacometti, Phys. Rev. E **72**, 011503 (2005).
[38] J. Köfinger, N. B. Wilding, and Gerhard Kahl, J. Chem. Phys. **125**, 234503 (2006).
[39] D. Gazzillo, J. Chem. Phys. **95**, 4565 (1991).
[40] E. Lomba, M. Alvarez, L. L. Lee, and N. G. Almarza, J. Chem. Phys. **104**, 4180 (1996).
[41] D. Kofke and E. Glandt, Mol. Phys. **64**, 1105 (1988).
[42] J. G. Amar, Mol. Phys. **67**, 739 (1989).
[43] K. Jagannathan, G. Reddy, and A. Yethiraj, J. Phys. Chem. B **109**, 6764 (2005).
[44] A. Neimark and A. Vishnyakov, Phys. Rev. E **62**, 4611 2000).
[45] R. Evans, U. M. B. Marconi, and P. Tarazona, J. Chem. Phys. **84**, 2376 (1986).
[46] E. Kierlik, M. L. Rosinberg, G. Tarjus, and P. Viot, Phys. Chem. Chem. Phys. **3**, 1201 (2001).
[47] L. D. Gelb, K. E. Gubbins, R. Radhakrishnan, and M. Sliwinska-Bartkowiak, Rep. Prog. Phys. **62**, 1573 (1999).
[48] W. F. Saam, J. Low Temp. Phys. **157**, 77 (2009).
[49] X. S. Chen, M. Kasch, and F. Forstmann, Phys. Rev. Lett. **67**, 2674 (1991).
[50] M. J. Blair and G. N. Patey, Phys. Rev. E **57**, 5682 (1998).
[51] G. M. Range and S. H. L. Klapp, Phys. Rev. E **70**, 031201 (2004).
[52] I. Szalai and S. Dietrich, Mol. Phys. **103**, 2873 (2005).
[53] N. G. Almarza, E. Lomba, C. Martin, and A. Gallardo, J. Chem. Phys. **129**, 234504 (2008).
[54] L. Li, L. Liang-Sheng, and C. Xiao-Song, Commun. Theor. Phy. **52**, 523 (2009).
[55] J. Puibasset, E. Kierlik, and G. Tarjus, J. Chem. Phys. **131**, 124123 (2009).
[56] P. Bartlett, P. R. H. Ottewill, and P. N. J. Pusey, J. Chem. Phys. **93**, 1299 (1990).
[57] Y. Hennequin, M. Pollard, and J. S. van Duijneveldt, J. Chem. Phys. **120**, 1097 (2004).
[58] Y. Yang, L. Liu, J. Zhang, C. Li, and H. Zhao, Langmuir **23**, 2867 (2007).
[59] C. Brunet, Ph.D. thesis, Université Paris-Est (Créteil), 2009.
[60] G. Bosma, C. Pathmamanoharan, E. H. A. de Hoog, W. K. Kegel, A. van Blaaderen, and H. N. W. Lekkerkerker, J. Colloid Interface Sci. **245**, 292 (2002).
[61] R. H. Ottewill, A. B. Schofield, A. B. J. A. Waters, and N. S. J. Williams, Colloid Polym. Sci. **275**, 274 (1997).
[62] J. Zhou, J. Ralston, R. Sedev, and D. Beattie, J. Colloid Interface Sci. **331**, 251 (2009); S. P. Stoylov, Colloids Surf., B **56**, 50 (2007).